CrossMark

High-temperature spin dynamics studied by solid-state nuclear resonance and electron paramagnetic resonance in ^{29}Si:B crystals

R. B. Morgunov[1] · O. V. Koplak[1,2]

Abstract The relaxation of nuclear magnetization in the ^{29}Si:B crystals obeys power-law kinetics at 300 K due to direct electron–nuclear relaxation. Admixture of the exponential relaxation associated with spin diffusion was revealed at higher temperatures. The inhomogeneous distribution of linear deformation defects was revealed by electron paramagnetic resonance. This factor mainly contributes to power-law kinetics of nuclear spin relaxation.

Introduction

Quantum information processing requires selective resonant control of multiple spin ensemble protected from thermal fluctuations [1, 2] Employing of the ^{29}Si nuclei in qubit technologies was proposed in [3, 4] In silicon crystals enriched with magnetic ^{29}Si isotope host atoms (nuclear spin $I_{Si} = ½$), electrical field controls over spin state of ^{31}P donor wave function [5], while quantum state might be decoded by nuclear magnetic resonance (NMR) and electron paramagnetic resonance (EPR) techniques [6]. Long spin correlation time of the ^{29}Si nuclear spins at room temperature (few hours) and long correlation time of ^{31}P electron spins (up to 1 min in [7]) allow qubit technology at room temperature. Dipole nuclear interaction [8] and electron–nuclear interaction governed by spins of paramagnetic defects [9] are the main driving factors of information processing in silicon crystals. Role of these factors was considered with an accuracy in Si:P crystals [7–10]. The ^{29}Si:B crystals are more complicate than ^{29}Si:P and they give a diversity of spin states due to high spin of the holes $S = 3/2$ and high nuclear spins of the stable boron isotopes $I = 3$ in ^{10}B and $I = 3/2$ in ^{11}B. In the ^{29}Si:B crystals, spin–orbital interaction separates spin levels of "light" and "heavy" holes. Mentioned above factors provide effective entanglement of quantum states and create more complicated structure of resonant spin transitions [6]. We have studied 2×10^{14} cm^{-3} boron-doped ^{29}Si crystals before and after their plastic deformation additionally introducing $\sim 10^{15}$ cm^{-3} paramagnetic deformation defects. Electron spin dynamics in undeformed (or under elastic deformation) silicon crystals of natural isotope abundance doped with boron was studied in [10–15]. Deformation defect possess strong localization of paramagnetic centers on dislocations in contrast with delocalized donor and acceptor wave functions. Spin states of the paramagnetic deformation defects were studied in ^{28}Si silicon crystals [16–19]. Linearity of the qubit disposition along dislocations is very important in the frame of technology of quantum computations proposed in [3, 4]. Creation of linear atomic chains by down-up building strategy is very complicate and expensive. Deformation defects (dislocations and linear assemblages of atoms in dislocation glide planes) are natural spin chains. This was a reason of our interest to examination of the possibility to use linear defects as quantum keys and to provide quantum processing in ^{29}Si:B silicon crystals. The aim of this paper is studying of kinetics of nuclear spin relaxation and contribution of the paramagnetic defects generated by plastic deformation to the electron–nuclear dynamics in ^{29}Si:B silicon crystals.

✉ R. B. Morgunov
morgunov2005@yandex.ru

1 Institute of Problems of Chemical Physics, 142432 Chernogolovka, Moscow, Russia

2 Taras Shevchenko Kiev National University and National Academy of Sciences, Kiev 01033, Ukraine

Experimental

Silicon crystals doped with boron ($\sim 2 \times 10^{14}$ cm^{-3}) were grown by float-zone technique. The crystal sizes were $a \times b \times c = 4 \times 16 \times 1$ mm^3 (the longer side b has [110] direction, 4×16 mm^2 plane is [111] a crystallographic plane). Concentrations of ^{28}Si, ^{29}Si, and ^{30}Si isotopes were 10, 75, and 15 %, correspondently.

The NMR spectra of micro powder samples (average size of milled powder particles was 45 μm) were recorded by a Bruker Avance III spectrometer. Magnetic field of a superconductive magnet was 9.4 T. Corresponding resonant frequency of ^{29}Si free non interacting nucleus was 79.5124 MHz. Pulsed sequence contained 90° pulses of 5 s duration. Signal detection "dead" time was 6.5 s. All spectra discussed in this paper are real parts of Fourier transform of free induction decay. Pause 2 h between spectra recording was observed for recovery of the initial zero spin polarization of nuclei.

Deformation paramagnetic defects in single crystals was revealed using a JOEL JES FA200 EPR spectrometer of the X—band frequency range (9.112 GHz). The modulation frequency was 100 kHz, sweeping magnetic field was in the range 0–8 kOe. Microwave power did not exceed ~ 1 mW to prevent saturation of the EPR transitions. The temperature was stabilized at 9 K with accuracy of ± 5 % in an ESR 900 Oxford Instruments cryostat. The first derivative of microwave power absorption dP/dH on magnetic field, H was considered as EPR spectrum. Rotation of the sample in the microwave cavity was carried out by goniometer with the relative error of ± 5 grad.

The ^{29}Si samples were deformed by the three-point bending around c axis at the 1223 K deformation temperature. Dislocation density n_d revealed by electron microscopy and chemical etching was $\sim 10^8$ cm^{-2}. Concentration of deformation paramagnetic centers was extracted from doubly integrated EPR spectra corresponding to spin susceptibility proportional to the amount of paramagnetic particles and spin factor $S(S + 1) = 7.5$. Comparison of magnetic susceptibility of deformation defects with that estimated in 0.1 mg of CuSO$_4$ 5H$_2$O reference sample results in $n \sim 10^{15}$ cm^{-3} concentration. This n value was larger than $n \sim a\, b\, \lambda\, n^{*}\, n_d = 10^{13}$ cm^{-3} obtained for typical linear concentration of the paramagnetic centers in the dislocation core $n^{*} \sim 10^7$ cm^{-1} and average size of the dislocation loop $\lambda \sim 10^{-2}$ cm [16–18]. Nevertheless, plastic deformation at high temperature 923 K generates large amount of paramagnetic clusters in the dislocation glide planes not associated with the dislocation core [16–18]. These clusters mainly contribute to EPR signal and nuclear relaxation in our experiments.

Results and discussion

NMR spectra interpretation

The NMR spectrum of the ^{29}Si reference sample at 300 K and its approximations by different methods are shown in Fig. 1. In [8], it was established that dipole–dipole nuclear interaction provides Lorentz shape of the NMR spectrum, if concentration f of ^{29}Si isotope is below 50 %. High concentration of ^{29}Si isotope $f = 75$ % results in Gauss line shape. In our crystals, where one can expect Gauss line shape. The comparison of the decompositions by four Lorentz and four Gauss lines is shown in Fig. 1. It is seen that Gauss shape is preferable for approximation in agreement with [8]. The NMR components were centered at -111.9 ± 0.3 ppm, -88.8 ppm ± 0.2, -78.4 ± 0.2 ppm, and -67 ± 2 ppm at $T = 300$ K.

^{29}Si nuclei exhibit chemical shifts from -60 ppm till -120 ppm in four-coordinated silicon. The -60 ppm chemical shift is typical for Si with no bridging oxygen, while more negative chemical shift is observed with increasing number of bridging oxygen atoms [20]. The peak at -111.9 ± 0.05 ppm corresponds to SiO$_2$ signal due to a quartz holder and silicon dioxide on the surface of the silicon micro particles.

The double-peak structure of the NMR spectra at -88.8 ± 0.1 and -78.4 ± 0.1 ppm is clearly observed in Fig. 1. Dipolar coupling between ^{29}Si spins in a nuclear ensemble is a main reason of these peaks splitting. The separation between the resonance lines depends on the dipolar coupling constant, R^{DD}, and the orientation Θ of the internuclear vector $\mathbf{r}_{ij}$ with respect to the applied magnetic field H in agreement with formula: [21]
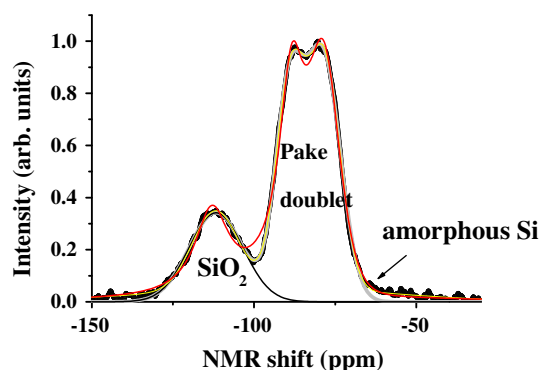

Fig. 1 NMR-MAS spectrum of ^{29}Si powder sample recorded at 300 K. Decomposition of the spectrum for SiO$_2$ line, Pake doublet and—67 ppm side peak is shown by *solid lines*: *yellow line* corresponds to approximation by 4 Gauss *shaped lines*, *gray line* corresponds to approximation by three Gauss *shaped lines*, and *gray line* corresponds to approximation by four Lorenz lines (Color figure online)

$$\Delta v = \tfrac{1}{2} R_{jk}^{DD}\left(3\cos^2\Theta - 1\right),\ R_{jk}^{DD} = \mu_0 \gamma_j \gamma_k h / 2\pi \langle r_{jk}\rangle^3$$

$$(1)$$

In a perfect silicon crystal lattice of the T_d point-group symmetry, every silicon atom has a tetrahedral environment due to four nearest neighboring atoms. All nuclear sites are magnetically equivalent since all Si–Si bonds are oriented along [111] crystallographic directions. Therefore, the effects of chemical shift anisotropy in NMR spectra can be neglected as well as zero quadrupolar interaction for ^{29}Si nuclear spin $I_{Si} = 1/2$. Direct and indirect nuclear dipolar interactions only contribute to the resonance spectra shape in silicon single crystals.

The long-range Ruderman–Kittel–Kasuya–Yosida (RKKY) interaction, and the short-range scalar coupling (J-coupling) can contribute to indirect dipolar interaction. The RKKY interaction is normally observed in NMR spectra of heavy doped semiconductors ($n > 10^{18}$ cm^{-3}) [10, 11]. In our samples, RKKY contribution to the linewidth of the resonance peaks can be neglected, because boron concentration was $\sim 2 \times 10^{14}$ cm^{-3} at $T = 300$ K. Direct magnetic dipolar interactions between two neighboring ^{29}Si nuclear spins in single ^{29}Si (99 %) crystal produces coupling up to 1000 Hz corresponding to the linewidth ~ 400 Hz (5 ppm) (Fig. 1a). The distance between these peaks in powder calculated by formula (1) averaged by Θ from 0 till 2π value should be $\Delta v/v = 3R^{DD}/2 = 7.5$ ppm ($\Delta v = 600$ Hz), which is in a good agreement with experimental value 7 ppm (Fig. 1a). Thus, direct dipole–dipole magnetic interaction is a main origin of the double peaks detected at -88.8 and -78.4 ppm. In the powder samples, where all orientations with respect to the applied magnetic field are represented, one can expect two additional side "knee-like" peaks corresponding to $\Theta = 90°$ orientation of the Si micro particles [21]. Separation of these peaks should be $3R^{DD} = 1200$ Hz corresponding to $\Delta v/v = 15$ ppm. No peaks centred at $-78.4 + 15/2 = -70.9$ ppm were observed in our experiments, probably because of very small amplitudes of these "knee-like" peaks. Instead of "knee-like" peaks at -70 ppm, a small wide peak centred at -67 ppm was found. The last one was absolutely necessary for correct spectrum decomposition. The absence of the peak at -67 ppm in approximation formula results in a strongly asymmetric Pake doublet extracted by approximation. Integral amplitudes of the doublet lines become up to ~ 2 times different between each other, if peak at -67 ppm is neglected. In the perfect silicon crystals, Pake doublet is symmetrical [21], because the shielding effect is negligibly small even if deformation defects are present. Thus, one can suppose that the -67 ppm peak originated from amorphous surface region of silicon micro-crystals.

Spin–lattice nuclear relaxation

Spin–lattice relaxation in ^{29}Si powder was studied after saturation of the spin system by a series of radiofrequency (RF) impulses. A measuring 90° impulse was applied after pause t to determine dependence of the nuclear magnetization I on pause t (Fig. 2a). The $I(t)$ function was not linear in semi logarithmic coordinates (see insert in Fig. 2a), while linear approximation of the $I(t)/I_0$ dependence was correct in the double-logarithmic coordinates (Fig. 2a). The comparison of the $I(t)/I_0$ curves obtained at 300 and 500 K demonstrates acceleration of spin relaxation at higher temperatures (compare Fig. 2a and b). Approximation of the $I/I_0(t)$ dependences by $I/I_0 = (t/t_0)^\alpha$ function results in parameters $\alpha = 0.63 \pm 0.013$, $t_0 = 83 \pm 2$ s at 300 K and $\alpha = 0.60 \pm 0.05$, $t_0 = 1 \pm 0.1$ s at 500 K. Although, power law was not an appropriate function at
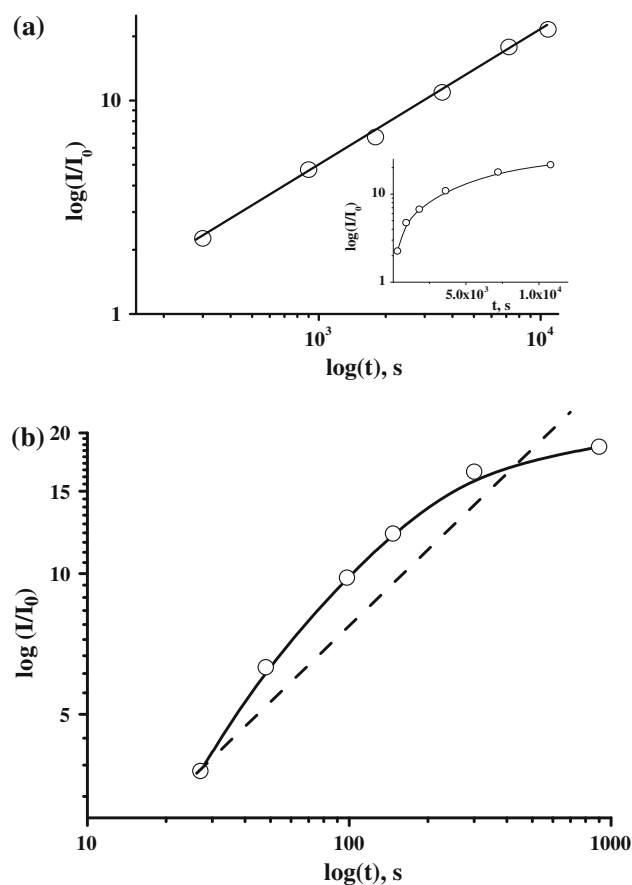

Fig. 2 a Time dependence of nuclear spin magnetization I normalized on its value I_0 at $t = 0$ in double-logarithmic coordinates at $T = 300$ K. The same dependence in semi logarithmic coordinates is shown in the insert. Solid line is approximation by function discussed in the text. b Time dependence of nuclear spin magnetization I normalized on its value I_0 at $t = 0$ in double-logarithmic coordinates at $T = 500$ K. Dashed line is approximation by power law, solid line is approximation by function discussed in the text

$T = 500$ K (Fig. 2b). The best approximation of the $I(t)/I_0$ dependence was obtained with the combined "exponential-power law" formula $I/I_0 = 1 - (t/t_0)^\alpha \, \exp(-t/T_1)$ (Fig. 2b). Increase of the temperatures causes acceleration of the spin–lattice relaxation. The approximation of the $I(t)/I_0$ dependence at 300 K results in parameters $\alpha = 0.63 \pm 0.04$, $t_0 = 80 \pm 3$ s. Approximation by the same function at $T = 500$ K results in $\alpha = 0.2 \pm 0.01$, $t_0 = 12 \pm 1$ s и $T_1 = 3812 \pm 30$ s parameters. Deviation of the nuclear relaxation kinetics from exponential function indicates negligibly small measurement time in comparison with saturation time.

The exponential dependence $I/I_0 = \exp(-t/T_1)$ is applicable to describe individual nuclear spins. Obviously, high concentration of the ^{29}Si isotope as well as the presence of paramagnetic centers in the studied crystals do not provide reliable isolation of the nuclear spins from each other and affect nuclear spin relaxation kinetics. Nuclear spin–lattice relaxation in crystals with paramagnetic centers involves two competing channels: direct relaxation by dipole–dipole coupling with the electronic spins of the paramagnetic centers and indirect relaxation provided by nuclear spin diffusion. The latter process is usually much faster in comparison with direct relaxation providing thermal equilibrium in the nuclear spin system. Rapid rotation of the sample at magic angle orientation can effectively quench spin diffusion [22]. Quenching is impossible in powder samples. Direct relaxation follows power-law behavior [23, 24]. On the contrary, relaxation controlled by spin diffusion is expected to follow exponential time dependence for homogeneous distribution of paramagnetic ions or a mixed power-law dependence for heterogeneous distribution of paramagnetic ions [25]. Thus, at $T = 500$ K both direct and indirect channels of nuclear spin relaxation are present, while direct electron-nuclear relaxation is dominant at $T = 300$ K in our experiments. Admixture of spin diffusion at $T = 500$ K is described by power factor α. Accordingly with theory of spin diffusion α should be equal to 0.5 in the case of isotropic spin relaxation [5]. Deviation of the α from classical value ($\alpha = 0.2$ at $T = 500$ K) indicates anisotropy of the spin diffusion probably caused by linear disposition of the paramagnetic centers created by plastic deformation [25]. Spin diffusion is determined by interrelation between radius of diffusion barrier δ and distance b corresponding to effective spin diffusion length. At high temperatures $b > \delta$ spin diffusion dominates (diffusion-limited relaxation), at low temperatures $b < \delta$ direct relaxation prevails (rapid diffusion). Thus, heating of the crystal from 300 to 500 K causes change of regime of the spin diffusion.

Temperature dependence of the NMR spectrum

Concentration of holes in Si:B remains unchanged with temperature in the 300–800 K range, because the hole thermal ionization energy of 0.045 eV corresponds to 460 K temperature. At $T > 400$–450 K most of acceptors are ionized. From the other side, intrinsic conductivity initiated by thermal fluctuation is negligibly small below 800 K. Thus, the chosen temperature range corresponds to charge carriers plateau on the concentration vs temperature curve. This circumstance is important for data analysis and comfortable for studying spin dynamics of charge carriers and nuclei.

The contribution of electron–nuclear dipole magnetic interaction to nuclear spin relaxation should be small in our crystals with acceptors concentration 2×10^{14} cm^{-3}, which is far from metal-like conditions. Additional electron spins appear in the crystals after plastic deformation. One could assume low effectiveness of the electron–nuclear
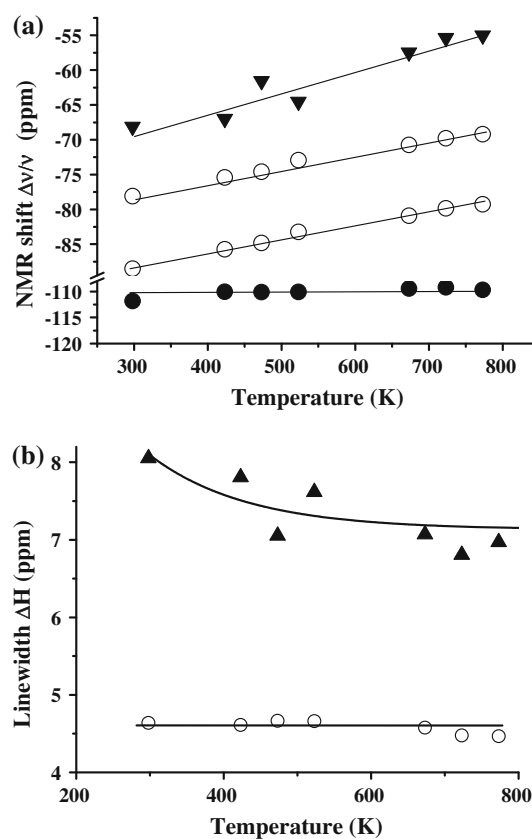

Fig. 3 Temperature dependences of chemical shifts (**a**) and linewidths (**b**) of ^{29}Si powder sample. Parameters of the Pake doublet are shown by *open circles*, chemical shift of SiO$_2$ fraction is shown by *closed circles*, parameters of—67 ppm *side line* are shown by *closed triangles*

spin relaxation channel. Nevertheless, we observe a strong temperature dependence of chemical shift of the lines belonging to Pake doublet (Fig. 3a). For that reason, we have applied a standard description of hole–nuclear interaction by Korringa expression including chemical shift $\Delta v/v$ and spin–lattice relaxation time T_1:

$$(\Delta v/v)^2 T_1 = h/2\pi k_B T(\gamma_h/\gamma_n)^2, \tag{2}$$

where γ_h and γ_n are holes and nuclear gyromagnetic ratios, correspondingly, k_B is Boltzmann constant. For ^{29}Si, the theoretical Korringa product $(\Delta v/v)^2 T_1 T$ is 6.67×10^{-6} s K. The substitution of $\Delta v/v$ values corresponding to the middle of the Pake doublet to Eq. (2) results in $T_1 = 9.05$ s at $T = 300$ K, and $T_1 = 5.43$ s at $T = 500$ K. The last one is far from $T_1 = 3812 \pm 30$ s determined from the exponential part of the nuclear spin relaxation (Fig. 2b). One can conclude that spin diffusion gives negligibly small contribution to the temperature dependence of the chemical shift. The main driving factor is direct electron–nuclear interaction including paramagnetic deformation defects. In spite of low concentration of the charge carriers, Korringa interaction contributes to nuclear spin relaxation governing the temperature dependence of chemical shift at high temperatures. Since NMR spectra were obtained in plastically deformed crystals, one can explain power-law and exponential parts of nuclear spin relaxation as contributions of the inhomogeneously distributed deformation paramagnetic defects and homogeneously distributed acceptors, correspondingly. The NMR linewidths in the Pake doublet were equal to each other and were temperature independent in the 300-800 K temperature range in contrast to temperature-dependent behavior of the line centered at -67 ppm at 300 K (Fig. 3b).

Effect of plastic deformation on EPR spectra

The presence of paramagnetic defects caused by plastic deformation was proved by EPR spectroscopy. A comparative analysis of the EPR spectra before and after plastic deformation shows additional lines appeared under stresses (Fig. 4).

Silicon crystals doped with boron contain "heavy" ($m_h = 0.49m_o$) and "light" $m_h = 0.16m_o$ holes (m_h is hole effective mass, m_o is free electron mass) [26]. These holes, both, form correspondent subbands split by spin-orbital and Zeeman interactions as shown in Fig. 4a. The intra- and inter- subband EPR transitions can be divided into two series: allowed transition with changing magnetic moment spin projection $\Delta m = 1$ and forbidden transitions $\Delta m = 2$ or 3, available for detecting [14, 15]. Figure 4b shows two survey ESR spectra measured at $T = 9$ K in the undeformed samples in [110] orientation and deformed ^{29}Si:B samples in [110] and [001] orientations of magnetic field.
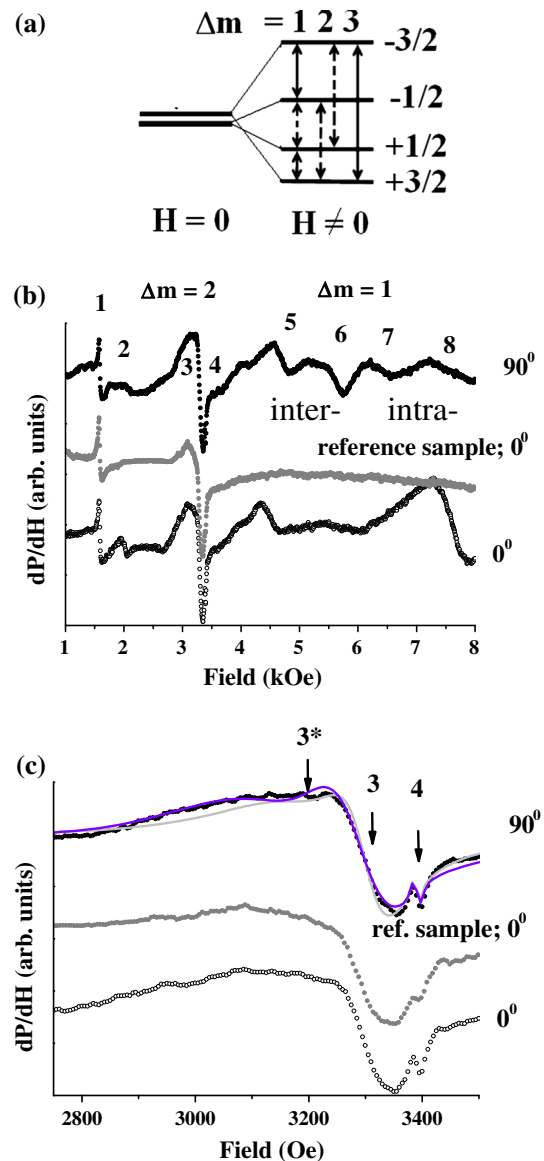

Fig. 4 a Scheme of allowed ($\Delta m = 1$) and forbidden ($\Delta m = 2, 3$) EPR transitions between split levels of "heavy" and "light" holes in Si:B single crystals. b EPR spectra of plastically deformed ^{29}Si:B single crystal in the orientations of magnetic field along (open circles) and perpendicular (closed circles) to [110] direction. EPR spectrum in the reference non-deformed sample is shown by gray symbols. c Fragments of the survey spectra shown in Fig. 4a and their approximations shown by blue line (Gauss peaks) and gray line (Lorentz peaks) (Color figure online)

In these spectra, there are few well-resolved B-related resonances. Accordingly to K. Itoh research [14, 15], the resonances at $H = 3297$ Oe and $H = 3391$ Oe (lines 3 and 4 are shown in the expanded scale in Fig. 4b) were assigned to a superposition of the two intersubband $\Delta m = 2$ transitions, where m is magnetic quantum number of the total angular momentum $J = 3/2$ of the B acceptor. The resonances at $H = 5730$ Oe and $H = 6220$ Oe

originate from a superposition of the two intersubband $\Delta m = 1$ transitions $|1\rangle \leftrightarrow |2\rangle$ and $|3\rangle \leftrightarrow |4\rangle$ and the intrasubband $\Delta m = 1$ transition $|2\rangle \leftrightarrow |3\rangle$, respectively. The series of the additional lines 3*, 4 not ascribed earlier is also observed in the spectrum of the deformed samples. The most remarkable difference between the spectra of the deformed and non-deformed crystals is the appearence of the complicate substructure containing lines 1–8.

Figure 4c shows approximation of the central fragment of the EPR spectra related to $\Delta m = 2$ transition. The Gauss approximation was much more accurate in comparison with the approximation by the Lorentz peaks. One can conclude inhomogeneous broadening of the EPR line. This fact is in good agreement with our conclusion on reasons of power–law nuclear spin relaxation caused by the inhomogeneous electron spin distribution. Linewidths of most of recorded EPR lines are strongly broadened and exceed the values calculated in the frames of electron–nuclear dipole interaction [14, 15]. Thus, acceptor traps as well as dislocation associated dangling bonds introduced by plastic deformation create the channel of nuclear spin relaxation with power-law kinetics. Lines 3*, 4 are isotropic and strongly broaden. One can not associate these lines with dislocations, because linewidths are larger and used temperatures are higher than usually observed in EPR corresponding to dislocation dangling bonds [17–19]. Plastic deformation generates not only dislocations. Linear chains of the clusters of the paramagnetic defects in the dislocation glide planes are also appearing under high temperature deformation. Contribution of different gliding systems provides different orientations of the clusters. For that reason, possible anisotropy of the EPR lines 3*, 4 is averaged by contributions of differently oriented defects and angular dependence is absent.

Magnetic field effect on aggregation of impurities in silicon crystals early reported in [27, 28] probably can not be observed in our experiments, because the float-zone crystals were studied. Magnetic field effects on impurity aggregation were observed in Czochralski silicon crystals containing oxygen only. We didnot detect any changes of EPR or NMR spectra due to field application.

Conclusion

Nuclear magnetization of Si^{29} crystals follows power-law kinetics at 300 K being admixed with an exponential contribution at higher temperatures. Power-law nuclear relaxation is provided by direct electron-nuclear relaxation of electron spins of deformation defects. The exponential part of relaxation is caused by nuclear spin diffusion associated with acceptors. Heating of the crystal from 300 to 500 K causes change of regime of the spin diffusion from rapid diffusion to diffusion-limited relaxation. Deformation defects detected by EPR mainly contribute to temperature dependence of chemical shift.

References

1. Hui HT (2006) Numerical method for determination of the NMR frequency of the single-qubit operation in a silicon-based solid-state quantum computer. Phys Rev B 74:195309
2. Zwanenburg FA, Dzurak AS, Morello A, Simmons MY, Hollenberg LCL, Klimeck G, Rogge S, Coppersmith SN, Eriksson MA (2013) Silicon quantum electronics. Rev Mod Phys 85:961–1019
3. Shlimak I, Safarov VI, Vagner ID (2001) Isotopically engineered silicon/silicon-germanium nanostructures as basic elements for a nuclear spin quantum computer. J Phys 13:6059
4. Itoh KM (2005) An all-silicon linear chain NMR quantum computer. Solid State Commun 133:747
5. Kane BE (1998) A silicon-based nuclear spin quantum computer. Nature 393:133–137
6. Simmons S, Brown RM, Riemann H, Abrosimov NV, Becker P, Pohl H, Thewalt MLW, Itoh KM, Morton JJL (2011) Entanglement in a solid-state spin ensemble. Nature 470:69–72
7. Stegner AR, Tezuka H, Riemann H, Abrosimov NV, Becker P, Pohl HJ, Thewalt MLW, Brandt MS (2011) Correlation of residual impurity concentration and acceptor electron paramagnetic resonance linewidth in isotopically engineered Si. Appl Phys Lett 99:032101
8. Hayashi H, Itoh KM, Vlasenko LS (2008) Nuclear magnetic resonance linewidth and spin diffusion in 29Si isotopically controlled silicon. Phys Rev B 78:153201
9. Hayashi H, Itahashi T, Itoh KM, Vlasenko LS, Vlasenko MP (2009) Nuclear magnetic resonance linewidth and spin diffusion in 29Si isotopically controlled silicon. Phys Rev B 80:045201
10. Fuller SE, Meintjes EM, Warren WW (1996) Impurity NMR study of the acceptor band in Si(B). Phys Rev Lett 76:2806
11. Sundfors RK, Holcomb DF (1964) Nuclear magnetic resonance studies of the metallic transition in doped silicon. Phys Rev 136:A810–A820
12. Neubrand H (1978) ESR from boron in silicon at zero and small external stress I. Line positions and line structure. Phys Status Solidi (b) 86:269–275
13. Bartelsen L (1977) The EPR fine structure spectrum of dislocations in silicon. Phys Status Solidi (b) 81:471–478
14. Stegner AR, Tezuka H, Andlauer T, Stutzmann M, Thewalt MLW, Brandt MS, Itoh KM (2010) Isotope effect on electron paramagnetic resonance of boron acceptors in silicon. Phys Rev B 82:115213
15. Tezuka H, Stegner AR, Tyryshkin AM, Shankar S, Thewalt MLW, Lyon SA, Itoh KM, Brandt MS (2010) Isotope effect on electron paramagnetic resonance of boron acceptors in silicon. Phys Rev B 81:161203(R)
16. Bagraev NT, Gusarov AI, Mashkov VA (1987) Spin-dependent processes in one-dimensional disordered dangling-bond systems in semiconductors. J Exp Theor Phys 92:548–549
17. Grazhulis VA, Ossipyan YuA (1971) Electron paramagnetic resonance of dislocations in silicon. J Exp Theor Phys 60:623–628

18. Weber ER, Alexander H (1983) Deep level defects in plastically deformed silicon. J Phys 44:C4-319–C4-328

19. Bagraev NT, Vlasenko LS (1982) Optical polarization of lattice nuclei in plastically deformed silicon. J Exp Theor Phys 83:1267–1274

20. Edèn M (2012) NMR studies of oxide-based glasses. Annu Rep Prog Chem Sect C 108:177–221

21. Verhulst AS, Maryenko D, Yamamoto Y, Itoh KM (2003) Double and single peaks in nuclear magnetic resonance spectra of natural and 29Si—enriched single-crystal silicon. Phys Rev B 68:054105

22. Devreux F, Boilot JP, Chaput F, Sapoval B (1990) NMR determination of the fractal dimension in silica aerogels. Phys Rev Lett 65:614

23. Sen S, Stebbins JF (1994) Phase separation, clustering, and fractal characteristics in glass: a magic-angle-spinning NMR spin-lattice relaxation study. Phys Rev B 50:822

24. Blumberg WE (1960) Nuclear spin-lattice relaxation caused by paramagnetic impurities. Phys Rev 119:79

25. Le Guennec P, Nechtschein M, Travers JP (1993) Nonexponential NMR relaxations in heterogeneously doped solids. Phys Rev B 47:2893

26. Feher G, Hensel JC, Gere EA (1960) Paramagnetic resonance absorption from acceptors in silicon. Phys Rev Lett 5:309

27. Skvortsov AA, Orlov AM, Gonchar LI (2001) The effect of a weak magnetic field on the mobility of dislocations in silicon. J Exp Theor Phys 93:117 **(Rus. Translated from Zhurnal Éksperimental'noi Teoretichesko Fiziki, 120(1):134–138, 2001)**

28. Yonenaga I, Takahashi K (2006) Effect of high-magnetic-field on dislocation-oxygen impurity interaction in Si. J Phys 51:407